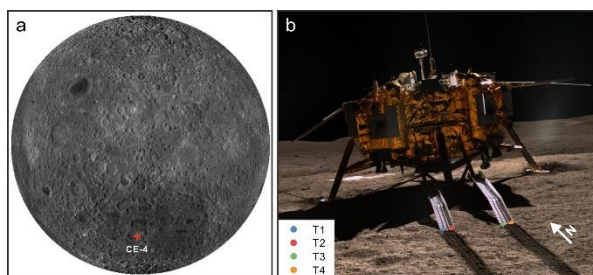


**THERMAL CONDUCTIVITY OF LUNAR REGOLITH AT CHANG'E-4 (CE-4) LANDING SITE.** X. Xiao<sup>1</sup>, S. Yu<sup>2</sup>, J. Huang<sup>1,4</sup>, H. Zhang<sup>3</sup>, Y. Zhang<sup>3</sup>, L. Xiao<sup>1</sup>, <sup>1</sup>State Key Laboratory of Geological Processes and Mineral Resources, School of Earth Sciences, Planetary Science Institute, China University of Geosciences, Wuhan 430074, China (xiaoxiao@cug.edu.cn), <sup>2</sup>State Key Laboratory of Lunar and Planetary Sciences, Macau University of Science and Technology, Macau SAR, China. <sup>3</sup>China Academy of Space Technology, Beijing 100094, China. <sup>4</sup>Chinese Academy of Sciences Center for Excellence in Comparative Planetology, Hefei 230026, China.

**Introduction:** Thermal conductivity of lunar regolith is critical for understanding the nature of lunar surface materials. Early works focused on estimating the thermal conductivity of lunar regolith through laboratory experiments on the Apollo regolith samples [1,2], but this method can only yield the condition at several landing sites with returned samples. Alternatively, the thermal conductivity of lunar regolith can also be estimated by the time-variation of surface temperature in the nighttime [3,4]. In this work, we are going to examine the thermophysical properties of lunar regolith at Chang'E-4 (CE-4) landing site based on the data of in-situ temperature probing experiment.

**Data:** The CE-4 lander landed at 45.4446°S, 177.5991°E, on the floor of von Karmen crater on January 3rd, 2019 [5]. After landing, Yutu-2 rover was released via the deployed two metallic rails orienting towards the south direction. Then, four temperature probes (T1—T4 in Figure 1b) beneath the end of two metallic rails began to measure the temperature of the topmost lunar regolith every 900 seconds. A detailed introduction to the payload and data acquisition can refer to ref. [6]. In this work, we select the temperature data obtained during the second and third lunar days after the landing, i.e. the UTC time 9:28:08, 27-February-2019 to 21:31:57, 29-March-2019 (Figure 2).



**Figure 1.** (a) Location of Chang'E-4 (CE-4) landing site. The mosaic of the lunar far side was obtained by Chang'E-1 (CE-1) charged-coupled device (CCD) camera. (b) The CE-4 lander on the lunar surface. The photo was taken by the Panorama Camera on the Yutu-2 rover in the local morning.

As a reference for comparison, we also evaluate the surface temperature during the daytime based on the thermal equilibrium on the lunar surface. For the

temperature data of all four probes, the climax is always lower than the theoretical value appearing near the local noon. Besides, the climax of surface temperature at T2 and T4 appears in the local morning, whereas the climax of surface temperature at T1 and T3 appears in the local afternoon. Both phenomena relate to the shading effect of lunar lander and metallic rails, which needs to be cautioned in the consequential analysis.

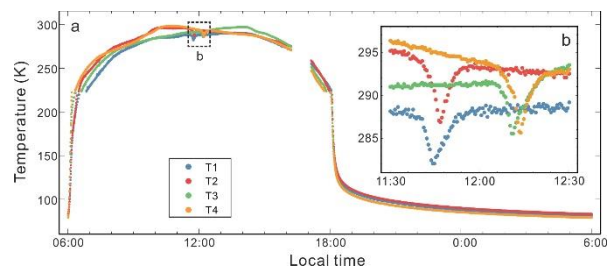


**Figure 2.** (a) The surface temperature at Chang'E-4 (CE-4) landing site probed by the temperature probes T1—T4 during the third lunar day after landing. (b) The temperature measured near the lunar noon of the third lunar day after landing.

**Results:** Owing to the better continuity over time, we select the temperature probed by the temperature probe T2 for analysing the thermal conductivity of the lunar regolith at CE-4 landing site. Heat conduction equation is used to simulate the diurnal variation of lunar surface temperature at CE-4 landing site. The density and thermal conductivity of lunar regolith are expressed in terms of grain radius and the external pressure associated with the load of metallic rails [7,8]. The heat capacity of lunar regolith is determined by a function of temperature suggested by the laboratory experiment for the regolith samples [9].

In order to achieve the best-fit between modeled surface temperature and probed surface temperature, the grain size at CE-4 landing site must be  $\sim 15 \mu\text{m}$  on average over depth. Correspondingly, our estimation yields a thermal conductivity of  $1.53 \times 10^{-3} \text{ W}/(\text{m}\cdot\text{K})$  on the surface and  $\sim 8.48 \times 10^{-3} \text{ W}/(\text{m}\cdot\text{K})$  at the depth of 1 m (Figure 3). The density of lunar regolith varies from  $651\text{--}865 \text{ kg}/\text{m}^3$  on the surface to  $1840 \text{ kg}/\text{m}^3$  at the depth of 5 m.

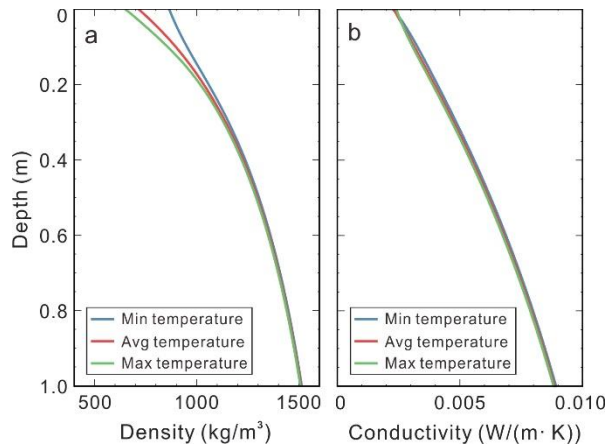


**Figure 3.** The profiles of density and thermal conductivity for the lunar regolith at Chang'E-4 (CE-4) landing site.

**Discussions and Conclusions:** The size of lunar regolith grains is an indicator to the degree of evolution associated with space weathering. In comparison with the geometric size of the samples collected at Chang'E-5 (CE-5) landing site, i.e.  $\sim 3.5\text{-}4.0\ \mu\text{m}$  [10, 11], the grain size at CE-4 landing site suggests a less mature regolith. Nevertheless, the age of CE-4 landing site, i.e.  $\sim 3.6\ \text{Ga}$  [12], is much older than that of CE-5 landing site, i.e.  $\sim 2.0\ \text{Ga}$  [13]. As a plausible explanation, the regolith below CE-4 landing site would be abnormally immature than that on the surface. This phenomenon is well consistent with an immature regolith layer at subsurface suggested by the spectral observations at Chang'E-3 (CE-3) landing site [14].

**Acknowledgments:** This work was supported by the National Key R&D Program of China (2021YFA0715100), the National Natural Science Foundation of China (42273041), the Pre-research Project on Civil Aerospace Technologies of CNSA (D020101, D020308, D020303) and the Fund for Development of Science and Technology of Macau SAR (0048/2020/A1).

**References:** [1] Cremers C. J. And Birkebak R. C. (1971) Proc. Lunar Sci. Conf. 2nd, 3, 2311-5. [2] Cremers C. J. and Hsia H. S. (1973) Proc. Lunar Sci. Conf. 4th, 4, 2459-64. [3] Yu S. And Fa W. (2016) PSS, 124, 48-61. [4] Hayne P. O. *et al.* (2015) LPSC 46th, 16-20. [5] Wu W. *et al.* (2019) Nature Geosci., 12, 222-3. [6] Sun Z. *et al.* (2022) Sci. Sin. Tech. 52. [7] Gundlach B. And Blum J. (2013) Icarus, 223, 479-92. [8] Schraepfer R. *et al.* (2015) Icarus, 257, 33-46. [9] Keihm S. J. (1984) Icarus, 60, 568-89. [10] Li C. *et al.*

(2022) *Natl. Sci. Rev.*, 9, nwab188. [11] Cao K. *et al.* (2022) *Sci. China Earth Sci.*, 65, 1704-14. [12] Huang J. *et al.* (2018) *JGR-Planets*, 123, 1684-700. [13] Che X. *et al.* (2021) *Science*, 374, 887-90. [14] Wu Y. And Hapke B. (2018) *EPSL*, 484, 145-53.